

Article

Au-Ag/TiO₂ Thin Films Preparation by Laser Ablation and Sputtering Plasmas for Its Potential Use as Photoanodes in Electrochemical Advanced Oxidation Processes (EAOP)

Luis Alejandro Martínez-Chávez ¹, Eric Mauricio Rivera-Muñoz ², Rodrigo Rafael Velázquez-Castillo ¹, Luis Escobar-Alarcón ^{3,*} and Karen Esquivel ^{1,*}

- ¹ División de Investigación y Posgrado, Facultad de Ingeniería, Universidad Autónoma de Querétaro, Cerro de las Campanas, Santiago de Querétaro 76010, Mexico; luisamch8mar@gmail.com (L.A.M.-C.); rodrigo.velazquez@uaq.mx (R.R.V.-C.)
- ² Centro de Física Aplicada y Tecnología Avanzada, Universidad Nacional Autónoma de México, A.P. 1-1010, Santiago de Querétaro 76000, Mexico; emrivera@fata.unam.mx
- ³ Departamento de Física, Instituto Nacional de Investigaciones Nucleares, Carr. México-Toluca S/N, Ocoyoacac 52750, Mexico
- * Correspondence: luis.escobar@inin.gob.mx (L.E.-A.); karen.esquivel@uaq.mx (K.E.); Tel.: +52-(55)-53297200 (ext. 12257 or 18041) (L.E.-A.); +52-442-192-12-00 (ext. 65401) (K.E.)



Citation: Martínez-Chávez, L.A.; Rivera-Muñoz, E.M.; Velázquez-Castillo, R.R.; Escobar-Alarcón, L.; Esquivel, K. Au-Ag/TiO₂ Thin Films Preparation by Laser Ablation and Sputtering Plasmas for Its Potential Use as Photoanodes in Electrochemical Advanced Oxidation Processes (EAOP). *Catalysts* **2021**, *11*, 1406. <https://doi.org/10.3390/catal11111406>

Academic Editors: Wonyong Choi, Detlef W. Bahnemann, Ioannis Konstantinou, Ewa Kowalska, Magdalena Janus, Vincenzo Vaiano and Zhi Jiang

Received: 29 October 2021

Accepted: 18 November 2021

Published: 20 November 2021

Publisher's Note: MDPI stays neutral with regard to jurisdictional claims in published maps and institutional affiliations.



Copyright: © 2021 by the authors. Licensee MDPI, Basel, Switzerland. This article is an open access article distributed under the terms and conditions of the Creative Commons Attribution (CC BY) license (<https://creativecommons.org/licenses/by/4.0/>).

Abstract: Titanium dioxide (TiO₂) is widely used, studied, and synthesized using different methodologies. By a modification of the material, it can be applied to wastewater treatment. A combined sputtering-laser ablation setup was used to deposit TiO₂ thin films modified, individually and simultaneously, with gold (Au) and silver (Ag). To investigate the effect of the metal incorporation in titanium and its impact on the photocatalytic activity, with dye discoloration as a pollutant compound model, the deposited films were characterized by UV-Vis, photoluminescence, and Raman spectroscopies, as well as by parallel beam X-ray diffraction. The results showed that films with different Au and Ag loads, and an 18 nm average crystallite size, were obtained. These metals have an essential effect on the deposited film's compositional, structural, and optical properties, directly reflected in its photocatalytic activity. The photocatalytic test results using UV-Vis showed that, after 1 h of applying a 4.8 V electric voltage, a discoloration of up to 80% of malachite green (MG) was achieved, using ultraviolet (UV) light.

Keywords: sputtering; laser ablation; thin films; titanium oxide; photo-electrocatalysis

1. Introduction

The preparation of thin films using plasma-based deposition systems represents an innovative route to prepare materials on a nanometric scale, with potential applications in different scientific research fields, such as renewable energy, photocatalysis, and water treatment [1,2]. Plasmas produced by laser ablation and magnetron sputtering have been widely used for thin film deposition, using different experimental setups. Nanomaterials, including thin films, have been studied in recent years because of their properties, which can differ significantly from the same material's properties in a bulk form. It is possible to prepare different thin films with thicknesses from a few, to hundreds, of nanometers by varying the deposition parameters. These techniques, based on the use of plasmas in some cases, have distinctive characteristics; for example, laser ablation has the advantage of congruent transfer, with which it is not necessary to use other reagents or chemical elements to obtain complex oxides with more than two cations in thin film form. On the other hand, the main advantages of the sputtering technique are high deposition rates, good uniformity, and easy control of the properties of the deposited films [3].

TiO₂ has been widely applied as a photocatalyst to mineralize non-biodegradable and recalcitrant chemical compounds into CO₂ and water under UV-light irradiation [4]. This

semiconductor has been used for nanopowders, nanorods, nanotubes, and in nanocomposites. It is worth mentioning that having the photocatalyst supported on a suitable surface avoids any subsequent separation process in the reaction system [5]. TiO₂ is a semiconductor that absorbs electromagnetic radiation in the UV region (e.g., <387 nm for the anatase phase), is amphoteric, and chemically stable [6]. It is widely used as a photocatalyst, due to its optical and electronic properties, relatively low cost, and low toxicity [7,8]. The anatase crystalline phase of TiO₂ exhibits photocatalytic activity; however, this is limited due to its low efficiency in the charge separation process when illuminated with visible light. Attempts to extend the photocatalytic activity of titanium oxide towards the visible region of the electromagnetic spectrum have been made by substituting Ti⁴⁺ in the TiO₂ lattice and incorporating metal ions as dopants, such as gold (Au), silver (Ag), platinum (Pt), and palladium (Pd) [9–13]. In addition, the combination of photocatalytic processes with the electrochemical ones, known as photo-electrocatalysis (PEC) [14], has been experimented with. In a PEC process the semiconductor is used as a photoanode, which is irradiated with light and simultaneously subjected to an external electric potential; in this way it is possible to induce charge separation of the electron/hole pairs (e⁻/h⁺), improving the catalytic process.

TiO₂ thin films grown using different deposition techniques, including thermal evaporation, sputtering, sol-gel, electrodeposition, chemical evaporation, and pulsed laser deposition, have been successfully obtained [3,15–21]. Laser ablation and magnetron sputtering techniques have been studied separately, as independent techniques to synthesize thin films of oxides [3,22–24]. Their combination of producing thin films by sputtering and their modification, by adding other elements such as metals through laser ablation, allows taking advantage of the intrinsic characteristics and advantages of these techniques. The use of hybrid configurations, in which the deposited material is formed by two independent plasmas produced from different targets, allows the possibility of modifying the plasma parameters independently, in a controlled manner [3]. Particularly, TiO₂ thin films modified with metals, non-metals, and coupled with other oxides in a controlled manner have been considered good alternatives for developing high-efficiency photocatalysts, with some key advantages, such as efficient charge separation and bandgap narrowing, thus, improving their photocatalytic performance using solar light [25]. Additionally, the combination of a noble metal with TiO₂ forms a Schottky barrier at the metal–semiconductor interface that works as an electron scavenger, reducing the photogenerated charge carrier recombination and consequently increasing the photocatalytic response [26].

Different studies have been reported successfully using such combinations, including TiO₂ based deposits [21]; TiC-Ag composites [27]; Co:TiO₂ and Bi:TiO₂ [3,28]; V₂O₅:Ag [29,30], for diverse applications. This research work aimed to use a hybrid deposition configuration by combining a sputtering plasma with a laser ablation plasma, to prepare and modify TiO₂ thin films with metals, as well as to evaluate their potential photocatalytic activity in the discoloration of malachite green (MG) dye in electrochemical advanced oxidation processes (EAOP), such as PEC.

2. Results and Discussion

2.1. Microstructural Characterization

Films with thicknesses around 48.4 ± 9.6 nm (average of seven measurements), as is shown in Figure 1, were obtained. This proved that the deposited materials consisted of thin films.

Parallel beam X-ray diffraction experiments were carried out to characterize the crystalline phase of the deposited materials. It can be seen in Figure 2 that crystalline materials were obtained. The diffraction patterns of the samples Au/TiO₂ and Ag/TiO₂ show the characteristic diffraction reflections of TiO₂ anatase phase at $2\theta = 25.3^\circ, 37.0^\circ, 38.6^\circ, 48.1^\circ, 53.9^\circ, 62.7^\circ$, (ICDD PDF#71-1166). Only one diffraction peak, attributed to the rutile phase at $2\theta = 27.5^\circ$, (ICDD PDF#75-1754), was found [31,32]. The standard diffractograms corresponding to the anatase and rutile crystalline phases of TiO₂ are included in Figure 2

as a reference. The Bragg reflections at $2\theta = 26.6^\circ, 33.9^\circ, 52.6^\circ, 54.6^\circ, 61.7^\circ, 65.7^\circ, 72.3^\circ,$ and 78.9° indicate the presence of tetragonal tin oxide, SnO_2 (ICDD PDF#46-1088) [33–35], corresponding to the ITO substrate. The peak at $2\theta = 37.8^\circ$ indicates the presence of gold and silver metallic particles (ICDD PDF#65-8601 and 65-8428, respectively) [32,36,37].

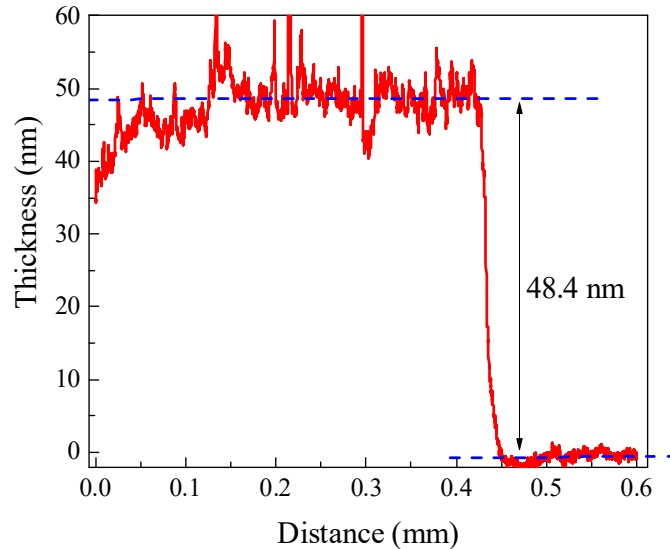


Figure 1. Thickness measured by profilometry of one of the deposited films.

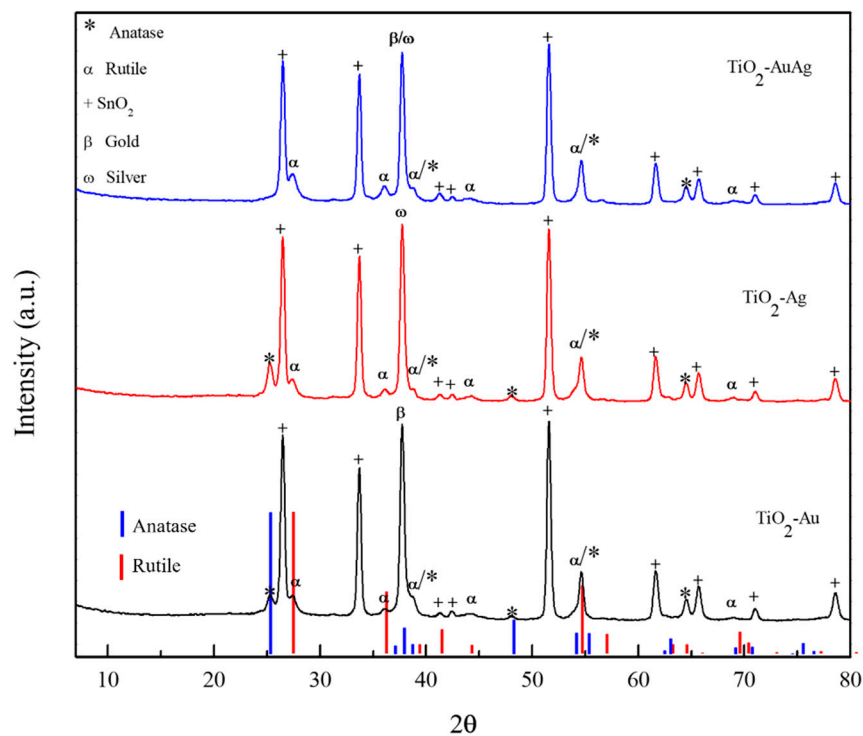


Figure 2. X-ray diffraction patterns of Au, Ag and AuAg-TiO₂ thin films.

The Williamson–Hall (W–H) method was used to calculate the crystallite size [38,39]. Figure 3 shows graphs of $\beta\text{Cos}\theta$ vs. $\text{Sin}\theta$ obtained by applying the proposed method. The average values of the Au, Ag, and Au–Ag crystallite size, determined from the intercept values ($K\lambda/D$), were 20, 17, and 17 nm, respectively.

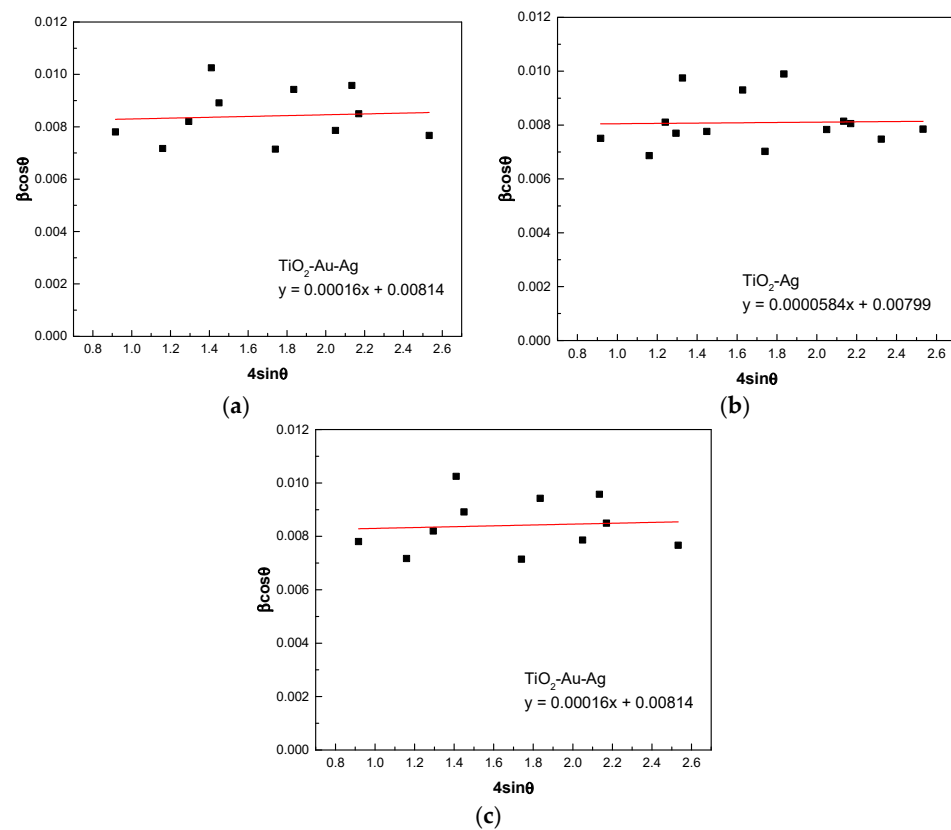


Figure 3. W–H analysis of TiO₂ metal-modified thin films (a) Au, (b) Ag, and (c) Au-Ag.

Figure 4 shows the Raman spectra obtained for the different samples. In all cases vibrational features at 143.3 cm^{-1} (E_g), 196.3 cm^{-1} (E_g), 397.1 cm^{-1} (B_{1g}), 517.4 cm^{-1} ($A_{1g} + B_{1g}$), and 638.6 cm^{-1} (E_g), characteristic of the TiO₂ anatase crystalline, were observed. No vibrational modes due to the rutile phase were detected [40,41].

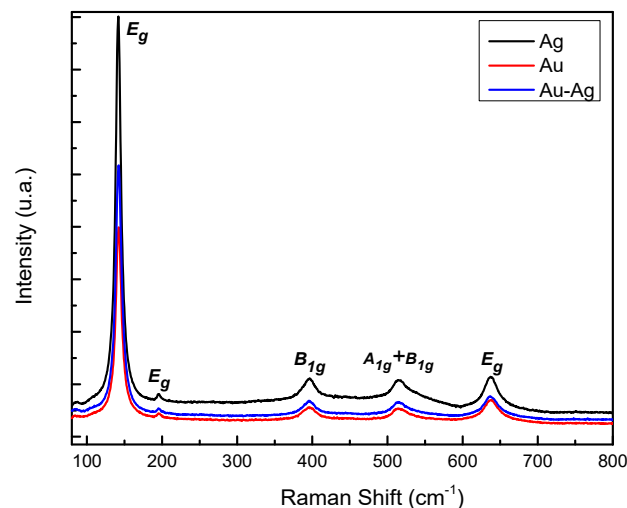


Figure 4. Raman spectra of TiO₂ Au, Ag, and Au-Ag modified thin films.

Figure 5 shows the vibrational mode corresponding to 517.4 cm^{-1} ($A_{1g} + B_{1g}$). It presents a clear broadening of the signal between 520 and 560 cm^{-1} ; previous studies attributed the presence of this signal (Figure 5b,c) to the presence of metallic gold on the surface of the thin film [21,41]. In the case of the film with silver, the signal broadening was lower than the corresponding signal of the films with Au (Figure 5a).

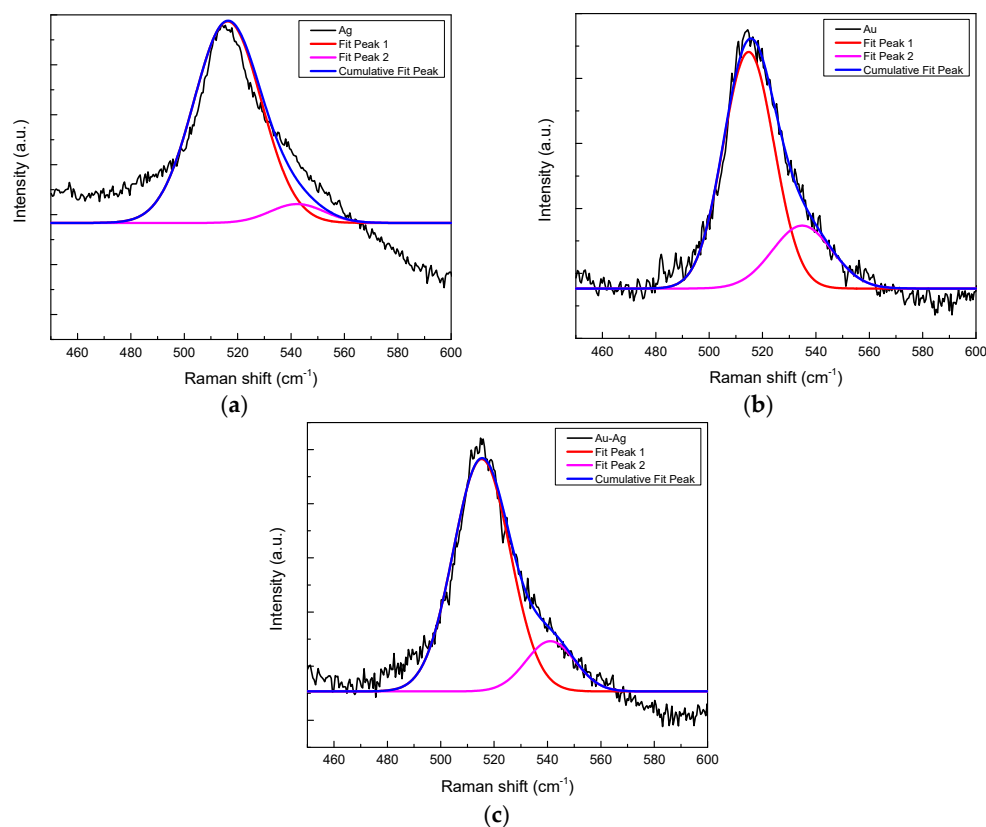


Figure 5. E_g Vibrational mode of TiO_2 in anatase phase at 537 cm^{-1} for (a) Ag, (b) Au and (c) AuAg modified thin films.

2.2. Optical Characterization

To determine the bandgap of the thin films and to know the nature of the metallic particles, UV-Vis measurements in the absorbance and transmittance modes were carried out. Figure 6a shows the absorbance spectra corresponding to the different thin films. For the samples Au/ TiO_2 and Ag/ TiO_2 , the presence of absorbance bands peaking at 557 nm and 441 nm is clearly observed, attributed to the surface resonance plasmons of Au and Ag, and indicating the presence of nanoparticles with spherical shapes and sizes in the nanometer scale; ranging 15–20 nm for Ag and 20–30 nm for Au. The spectrum corresponding to the sample with Au-Ag does not show defined absorbance band peaks, probably due to the lack of spherical nanoparticle formation [11,32,42,43].

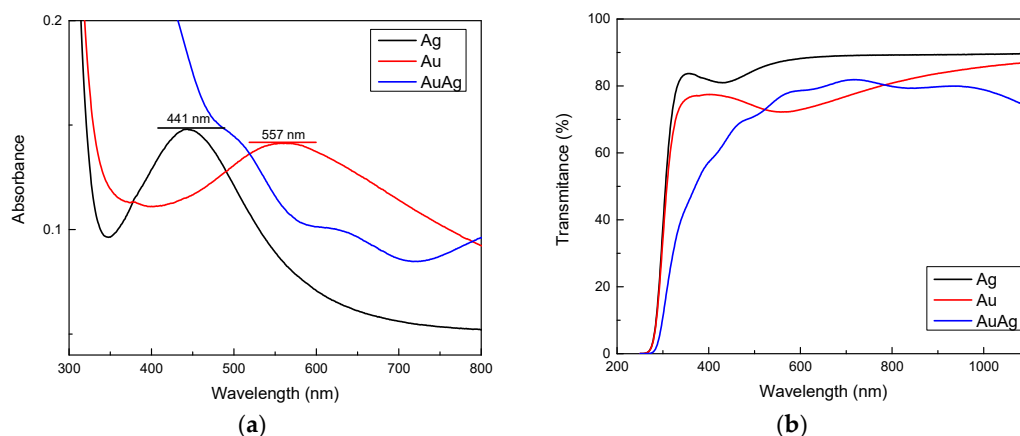


Figure 6. Cont.

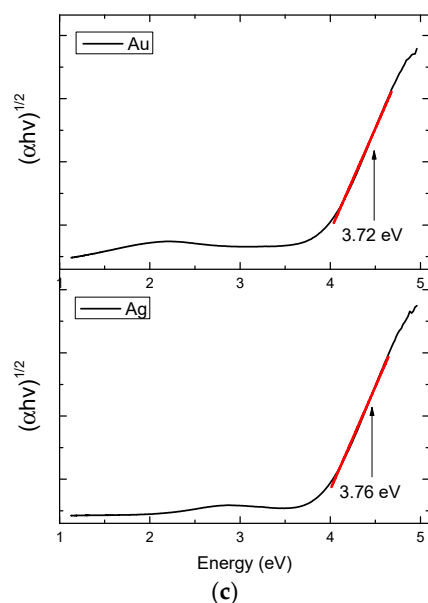


Figure 6. (a) Absorbance, (b) transmittance spectrum, and (c) Tauc plots for thin films Au, Ag, and Au-Ag-TiO₂.

Figure 6b shows the transmittance spectra of the thin films. A red shift of the absorption edge for the Au-Ag/TiO₂ is observed. The bandgap was determined using the Tauc method, assuming indirect transitions due to the nature of the semiconductor (Figure 6c); this was plotted $(\alpha h\nu)^{1/2}$ as a function of the photon energy. E_g values were obtained by a linear fit of the linear portion of the curve, determining its intersection with the photon energy axis as the quotient of the intercept to the slope. The obtained E_g values were 3.72 eV for the thin film with Au, and 3.76 eV for the film with Ag. The higher bandgap values of metal-modified TiO₂ thin films compared to the bulk TiO₂ bandgap value can be attributed to the thickness of the thin film, which modifies the optical properties, and it is not possible to observe well-defined interference patterns in the transmittance spectrum (Figure 6b); therefore, the thin film behaves as a kind of electrical insulator. Consequently, the photon effect over the surface causes a bandgap shift, requiring higher energy to be activated [21].

The presence of Ag and Au in the form of nanoparticles was corroborated through transmission electron microscopy (TEM); due to the joint between the thin film and the substrate meaning they could not be analyzed together, the Ag and Au samples were deposited directly on copper TEM grids under the same laser ablation conditions mentioned in the experimental section. Figure 7a corresponds to the Ag nanoparticles, showing quasi-spherical shapes with an average particle size close to 13 nm. Figure 7b corresponds to the Au nanoparticles with a completely different shape, which could have been formed by quasi-spherical particles forming linear agglomerates. The observed sizes are in good agreement with the wavelength position of the surface plasmons discussed in the UV-Vis results (Figure 6a). Therefore, it can be inferred that the thermal process did not modify the metallic particles deposited by ablation over the thin films [32,43,44].

Figure 8 shows the photoluminescence emission spectra obtained for the thin films prepared in this work. In general terms, it is observed that the spectra have the same shape and broadening for each thin film. Four major features can be distinguished in these spectra. The shoulder in the wavelength interval from 375 to 400 nm (3.3 to 3.1 eV) may be attributed to band to band transitions related directly to the bandgap [2,45]. On the other hand, the signal between 430 and 450 nm (2.9 to 2.7 eV) may be associated with the production of excitons (electron-hole pairs) generated by the excitation energy.

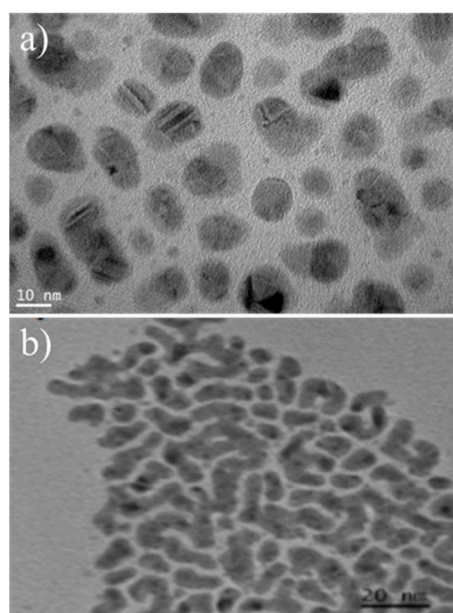


Figure 7. Transmission electron microscopy (TEM) images of Ag (a) and Au (b) nanoparticles.

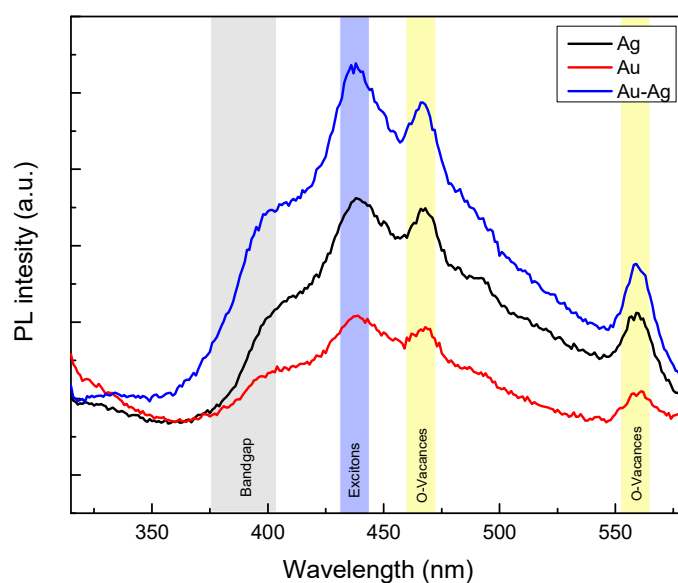


Figure 8. Photoluminescence spectra of TiO₂ films with Ag, Au, and Au-Ag nanoparticles.

Finally, the emissions observed in the wavelength interval between 450–475 nm (2.7 to 2.6 eV) and 550–575 nm (2.2 to 2.1 eV) can be attributed to the surface states of oxygen vacancies in TiO₂ in its anatase phase [21,46]. Additionally, the differences in emission intensity reveals that metal modification changes the recombination rate of the electron-hole pairs. The thin film with Au shows a lower recombination rate, while the thin film with the simultaneous presence of Au and Ag, seems to favor the recombination process.

2.3. Photoelectrocatalytic Experiments

Figure 9 shows the absorbance spectrum corresponding to the malachite green dye at 50 mg/L concentration. The bands peaking at 617, 427, and 317 nm are characteristic of malachite green dye [47]. The band responsible for the color is the most intense, located at 617 nm in the spectrum [48,49].

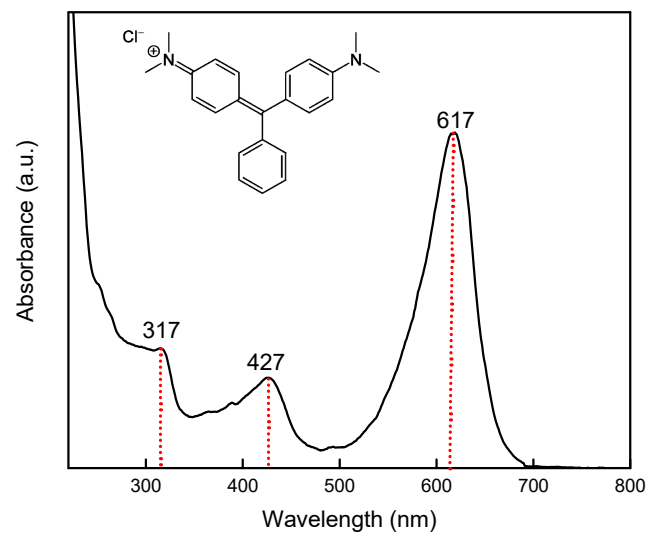


Figure 9. Absorbance spectrum of malachite green dye.

Figure 10 shows the obtained results from the electro and photo-electrocatalytic experiments for each of the thin films (photoanodes). The experiments were carried out with and without light irradiation (PEC and EC, respectively). The degradation of malachite green dye using the three photoanodes was satisfactory. In the EC experiments the lowest color removal, close to 45%, was obtained with the Ag/TiO₂ film; followed by the Au/TiO₂ film, with 60% of color removal; the maximum of 70% being obtained with the Ag-Au/TiO₂ film in a total reaction time of 60 min. Concerning the photo-electrocatalytic experiment (PEC), the Ag/TiO₂ and Ag-Au/TiO₂ films reached approximately the same discoloration degree, close to 75%, while the thin film of TiO₂-Au achieved a maximum degradation of 84% at the same time. These results for the percentage of MG discoloration are directly related to the obtained PL results, because the thin film with Au showed a lower recombination rate of electron-hole pairs, contributing to the TiO₂ mechanism for organic molecule degradation [4,21,29].

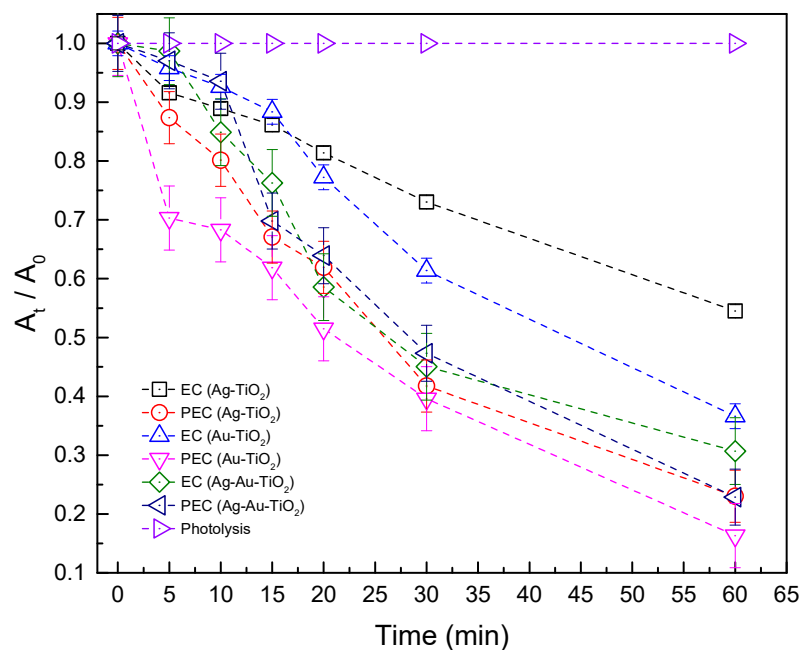


Figure 10. Comparison of color removal of malachite green dye solution at pH = 1 by the photoanodes in the EC and PEC tests.

The results showed that an electric voltage applied directly affects the discoloration process when using a semiconductor as anode [21,31], due to the fact that in the photolysis process no discoloration of the solution was observed, as expected. On the other hand, the irradiation with UV light facilitated the EC experiments, by contributing to the color disappearance process, in which, as a result, better discoloration was obtained than when the experiments were performed without the application of UV light.

The three bands corresponding to malachite green at 617, 427, and 317 nm were noticeably diminished in their intensity with the electric voltage (Figure 11a) and, in the presence of electromagnetic radiation in the form of ultraviolet light combined with the electric voltage (Figure 11b), with the three photoanodes. More kinetic studies and measurements of the mineralization of MG are needed to confirm if these photoanodes are capable of achieving complete CO₂ and H₂O formation from the dye MG molecules. Nevertheless, as can be observed from the discoloration test, the Au-TiO₂ photoanode showed remarkable properties and can be considered a functional photoanode for advanced electrochemical oxidation processes, leading the prospect of having a novel formation route for this supported catalyst.

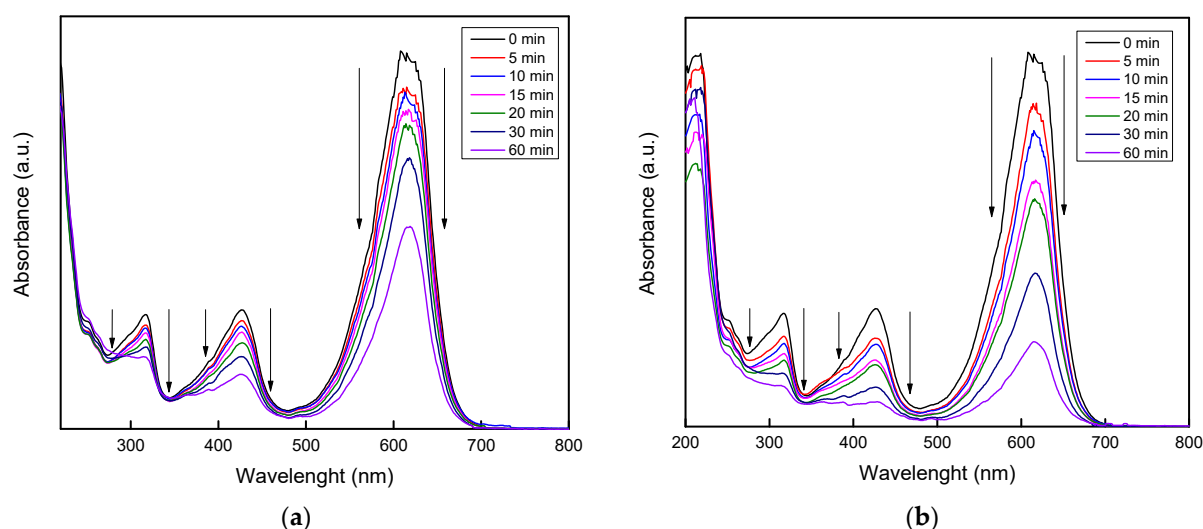


Figure 11. Absorbance spectra of MG dye using the Ag-TiO₂ photoanode through (a) EC and (b) PEC processes at different reaction times.

The data shown in Figure 12 were used to plot $\ln(A/A_0)$ vs. time. A pseudo-first-order kinetic model was fit to these plots [50]. Figure 12a,b show good linear fits for all samples, with constant rates from 0.00987 to 0.2595 min⁻¹ (Table 1). For the EC experiments it can be seen that the load of silver and gold in the Ag-Au-TiO₂ photoanode facilitated the discoloration process compared to the single metal TiO₂ photoanode modification. Nevertheless, for the PEC experiments, the Au-TiO₂ photoanode result in the highest kinetic reaction constant (0.02867 min⁻¹), but like the rest of the photoanode materials, further studies regarding the electric properties of the photoanodes are proposed, to fully understand how the incorporation of a single or combined metallic nanoparticle in the TiO₂ thin film could modify the donor concentration, due to the oxygen vacancies, or the interfacial electron transfer [51].

Table 1. Rate constant (K_{Obs}) values for the different photoanodes applied to EC and PEC processes.

Sample	K_{Obs} (min ⁻¹)	Sample	K_{Obs} (min ⁻¹)
TiO ₂ -Ag (EC)	0.00987	TiO ₂ -Ag (PEC)	0.025
TiO ₂ -Au (EC)	0.01756	TiO ₂ -Au (PEC)	0.02867
TiO ₂ -Ag-Au (EC)	0.02124	TiO ₂ -Ag-Au (PEC)	0.02595

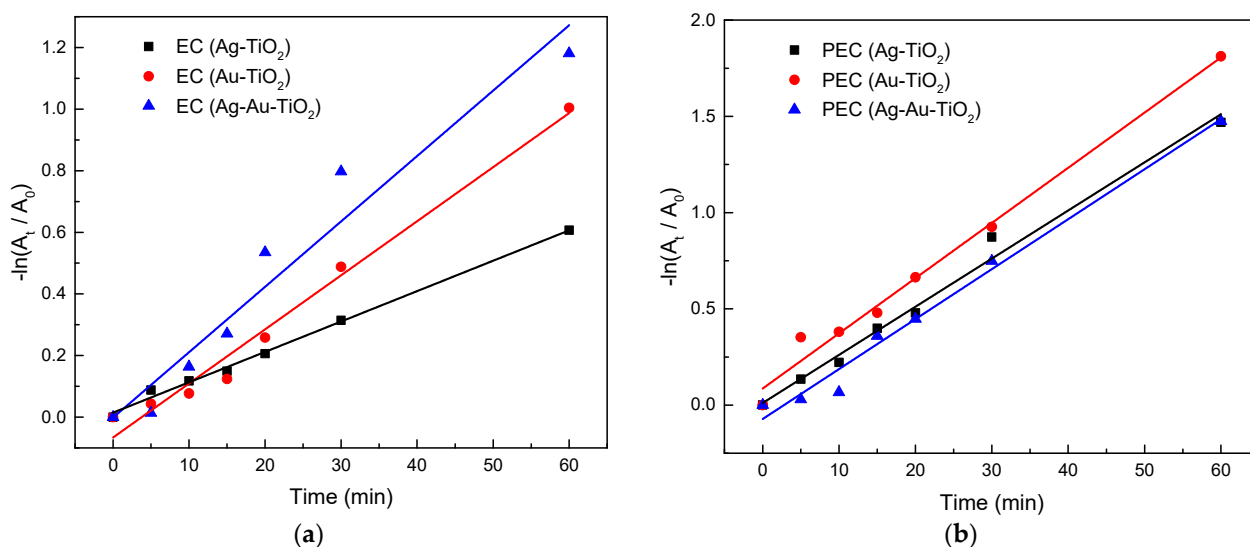


Figure 12. Pseudo-first-order kinetic fit of (a) EC and (b) PEC discoloration test of 50 ppm MG at 60 min.

The degree of electrochemical enhancement (E) and the degree of process synergy (S) were calculated using Equations (1) and (2), as reported by [52,53].

$$E = (K_{PEC} - K_{PC})/K_{PEC} \quad (1)$$

$$S = (K_{PEC} - (K_{PC} + K_{EO}))/K_{PEC} \quad (2)$$

where K_{PEC} , K_{EO} , and K_{PC} are the apparent rate constants for the photo-electrocatalytic, electrochemical, and photocatalytic degradation of MG. For all photoanodes, the process synergy was $(S) > 0$, confirming that the improved performance obtained with PEC degradation is more than a simple addition of the individual EC and photocatalytic degradation processes. For Ag-TiO₂, Au-TiO₂, and Ag-Au-TiO₂ thin films, the S values were 0.01, 0.39, and 0.18, respectively. The calculated E values were 40% for the Ag-TiO₂ film, whereas for the Au-TiO₂ and Ag-TiO₂ in both cases they were >90%. These results are in good agreement with those observed in the kinetic analysis and discoloration tests.

To the best of our knowledge, there has been no previous work that used a hybrid system of laser ablation and sputtering for the formation of thin films of TiO₂ modified with noble metals such as Au and Ag. The use of the proposed hybrid deposition system takes advantage of the qualities of each of these techniques for the formation of thin films, with potential applications in photo-electrocatalytic processes (PEC), as revealed in the results presented in this work.

There have been several different works where thin films were obtained with similar methods and used in PEC processes. Nevertheless, only the photocatalytic process was evaluated, with high-power lamps (compared to that of the present work), wavelengths close to the UVC range (greater than the range handled in this work), a greater electrode work area, and also with relatively low concentrations of pollutant in the water (up to a couple of orders of magnitudes less than in the present work) and longer reaction times [2,3,21,54–57].

3. Materials and Methods

3.1. Thin Films Preparation

TiO₂ thin films deposited by magnetron sputtering were modified by the incorporation of Au and Ag, using the laser ablation technique. This experimental setup had been used in previous works with interesting results [1,2,21]. The base pressure was approximately 5×10^{-5} Torr, and the working pressure was set at 2×10^{-2} Torr of argon of high purity. A titanium target (purity 99.99%, Kurt J. Lesker Company, Jefferson Hills, PA, USA 2")

diameter and 0.25" thickness, was sputtered at a power of 150 W. Films were deposited on ITO (indium and tin oxide) substrates (1 × 1 inch, prepared using a ITO target, purity 99.99%, Kurt J. Lesker Company, Jefferson Hills, PA, USA) kept at room temperature. The target to substrate distance was 12.5 cm, and the deposition time was 30 min.

Figure 13 shows schematically the setup used to deposit the metals by laser ablation. In this case, Au and Ag targets (high purity, 99.99%, Kurt J. Lesker Company, Jefferson Hills, PA, USA), 1" diameter and 0.25" thick, were used. The third harmonic (355 nm) of a Nd:YAG laser (Q-Smart 850, Quantel, Lannion, France) was used as an energy source, focusing the laser beam using a 30-cm focal length plano-convex lens. The target to substrate distance was 7 cm. The target was rotated with an electric motor to avoid depletion of material at any given spot. After deposition of the Ti film, the vacuum chamber was evacuated to the base pressure to incorporate simultaneously the gold (Au/TiO₂), silver (Ag/TiO₂) and Au-Ag (Au-Ag/TiO₂) nanoparticles on the Ti film. The ablation conditions were energy per laser pulse of 18 mJ (1000 pulses) for gold and 25 mJ (7000 pulses) for silver. After deposition, the films were subjected to a thermal treatment at 450 °C for two hours, to promote the growth of the anatase crystalline phase through thermal oxidation. We expected to obtain the anatase phase after the thermal treatment, which is well known as a catalyst for reduction–oxidation reactions for organic chemical compound removal.

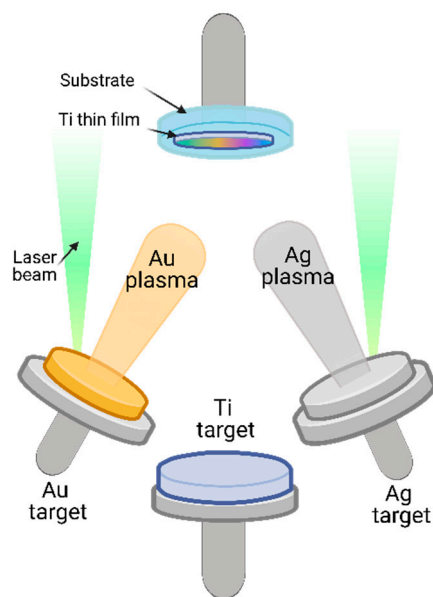


Figure 13. Titanium thin film (Ti) modification by Au and Ag.

3.2. Thin Films Characterization

The microstructure of the films was studied using Raman spectroscopy; the spectra were obtained using a micro-Raman system (LabRam HR 800, Horiba Jobin Yvon, France), equipped with a confocal microscope (Olympus BX40, Olympus Corporation, Pennsylvania, USA); the samples were analyzed using a wavelength of 532 nm at a power close to 1 mW. The crystalline structure of the deposited thin films was determined by a X-ray diffraction system (Rigaku Ultima IV Diffractometer, Rigaku Corporation, Texas, USA), with the Cu K α radiation line ($\lambda_k = 1.5406 \text{ \AA}$) operated at 40 kV and 30 mA. The diffraction patterns were recorded using a parallel beam in a 2 θ configuration. The incident parallel beam was fixed at 2° from the sample surface, acquiring data from 2 $\theta = 5$ to 80° with a Solid-State Detector (D/teX-ULTRA, Rigaku Corporation, Texas, USA) at a speed of 1°/min and a sampling time of 0.02 sec. The photoluminescence properties of the thin films were studied using PL spectroscopy, using a spectrofluorometer (FluoroMax 4, Horiba Jobin Yvon, France) equipped with a 150 W Xenon lamp as excitation source. The optical

absorbance and transmittance of the thin films were measured with a Spectrophotometer (Lambda 35, PerkinElmer, Waltham, MA, USA), from 200 to 800 nm.

3.3. Photoanodes Preparation and Photoelectrocatalytic Experiments

Photoanodes were formed by cutting a piece of the thin film (1 cm^2) and attaching it to a copper wire, using silver paint as electrical contact. The electrical connection between the film and the copper wire was coated with epoxy resin to avoid the copper wire from reacting with the solution inside the photoelectrochemical cell. The photo-electrocatalytic experiments were carried out in a photoelectrochemical cell, which consisted of a Teflon container of 15 cm^3 with a quartz window to allow the UV light (404 nm) to focus directly on the photoanode. During the experiments, air bubbling flow (1 L/min) and constant stirring were used. Graphite was used as cathode for the experiments.

The photo-electrocatalytic activity of the thin films (Au/TiO_2 , Ag/TiO_2 , and Au-Ag/TiO_2) was evaluated by monitoring the discoloration of malachite green (MG) dye at different reaction times (5, 10, 15, 20, 30, and 60 min). A MG solution of 50 mg/L was prepared with Na_2SO_4 (0.5 mM) as electrolyte in an acid environment ($\text{pH} = 1$ adjusted with H_2SO_4 , 95–98% JT Baker). The discoloration was evaluated by applying an electric voltage of 4.8 V with a Triple output DC power supply $0\text{--}6 \text{ V}$, $5\text{A}/0 \pm 25 \text{ V}$, 1A (Keysight E3631A, Keysight Technologies, California, USA) in the presence and absence of light using a UV-lamp (365 nm), and with a distance between the window cell and the light source of 10 cm [21,58]. Photolysis and photocatalytic reactions were performed to compare the discoloration obtained for the electro- and photo-electrocatalytic systems. Dye degradation was followed by a decrease of the characteristic MG absorption band at 616 nm , as a function of the reaction time.

4. Conclusions

Using an alternative deposition method, combining two different plasma deposition techniques, it was possible to obtain semiconductor thin films based on TiO_2 modified with Au, Ag, and Au-Ag, with potential applications in advanced electrochemical oxidation processes (EAOP), to remove non-biodegradable and emerging organic pollutant compounds. The physical and chemical characterization of the prepared materials showed a crystalline material with a suitable phase to carry out the photocatalysis process. The UV-Vis results and TEM images confirmed the presence of metallic Au and Ag nanoparticles on the TiO_2 thin films, with sizes close to 13 nm for the Ag particles. The photoluminescence spectroscopy results revealed different emission bands corresponding to exciton generation, the oxygen surface states, and the bandgap in the anatase phase in the thin film form. In the malachite green dye photo-electrocatalysis tests, it was possible to achieve a maximum 84% color removal after 60 min under UV radiation, applying a 4.8 V electric potential. From the kinetic analysis and the calculation of the degree of electrochemical enhancement (E) and the degree of process synergy (S), it was possible to assess the color removal results and to set a precedent for subsequent studies regarding the electronic properties of thin films.

Furthermore, as future work, we plan to study the mineralization and degradation of the MG molecule, comparing the photo-electrocatalytic process with other EAOP, such as the electro-Fenton (EF) and photoelectro-Fenton (PEF) methods.

Author Contributions: Conceptualization: K.E.; Methodology: K.E., L.A.M.-C. and L.E.-A.; Formal analysis and investigation: K.E., L.A.M.-C., E.M.R.-M., R.R.V.-C. and L.E.-A.; Writing—original draft preparation: L.A.M.-C.; Writing—review and editing: K.E., L.A.M.-C., E.M.R.-M., R.R.V.-C. and L.E.-A.; Funding acquisition: K.E. and L.E.-A.; Resources: K.E., E.M.R.-M., R.R.V.-C. and L.E.-A.; Supervision: K.E. and L.E.-A. All authors have read and agreed to the published version of the manuscript.

Funding: This research received financial grant from FONDEC-UAQ-2021 through the Research Project [FIN202116] and from the fund Investigación Vinculada a la Atención de Problemas Nacionales 2021-FI through the Research Project [FIN202106].

Data Availability Statement: The data presented in this study are available on request from the corresponding authors.

Acknowledgments: L.A.M.-C. thanks CONACyT for the scholarship granted (CVU. No. 815785). Authors thank Beatriz Millán-Malo for technical support in XRD analysis and acknowledge the facilities of the Laboratorio Nacional de Caracterización de Materiales (LaNCaM).

Conflicts of Interest: The authors declare no conflict of interest.

References

1. Escobar-Alarcon, L.; Solís-Casados, D.A.; González-Zavala, F.; Romero, S.; Fernandez, M.; Haro-Poniatowski, E. Preparation of Nanostructured Bi-Modified TiO₂ Thin Films by Crossed-Beam Laser Ablation Plasmas. In *Proceedings of the Journal of Physics: Conference Series*; Institute of Physics Publishing, IOP publisher: London, UK, 2017; Volume 792, p. 012006.
2. Escobar-Alarcón, L.; Gonzalez-Zavala, F.; Solis-Casados, D.A.; Fernandez, M.; Aspiazú, J.; Haro-Poniatowski, E. Zn-Modified TiO₂ Thin Films Deposited by Combining Plasmas Produced by Laser Ablation and Magnetron Sputtering. *Appl. Phys. A Mater. Sci. Process.* **2018**, *124*, 1–7. [[CrossRef](#)]
3. Escobar-Alarcón, L.; Solis-Casados, D.A.; Romero, S.; Haro-Poniatowski, E. Thin Films Prepared by a Hybrid Deposition Configuration Combining Two Laser Ablation Plasmas with One Sputtering Plasma. *Appl. Phys. A Mater. Sci. Process.* **2020**, *126*, 1–8. [[CrossRef](#)]
4. De Santiago Colín, D.M.; Martínez-Chávez, L.A.; Cuán, Á.; Elizalde-Peña, E.A.; Rivera, J.A.; Guzmán, C.; Escobar-Alarcón, L.; Esquivel, K. Sonochemical Coupled Synthesis of Cr-TiO₂ supported on Fe₃O₄ structures and Chemical Simulation of the Degradation Mechanism of Malachite Green Dye. *J. Photochem. Photobiol. A Chem.* **2018**, *364*. [[CrossRef](#)]
5. Silva, T.A.; Diniz, J.; Paixão, L.; Vieira, B.; Barrocas, B.; Nunes, C.D.; Monteiro, O.C. Novel Titanate Nanotubes-Cyanocobalamin Materials: Synthesis and Enhanced Photocatalytic Properties for Pollutants Removal. *Solid State Sci.* **2017**, *63*, 30–41. [[CrossRef](#)]
6. López, R.; Gómez, R.; Oros-Ruiz, S. Photophysical and Photocatalytic Properties of TiO₂-Cr Sol-Gel Prepared Semiconductors. *Catal. Today* **2011**, *166*, 159–165. [[CrossRef](#)]
7. Fang, J.; Cao, S.-W.; Wang, Z.; Shahjamali, M.M.; Loo, S.C.J.; Barber, J.; Xue, C. Mesoporous Plasmonic Au-TiO₂ Nanocomposites for Efficient Visible-Light-Driven Photocatalytic Water Reduction. *Int. J. Hydrog. Energy* **2012**, *37*, 17853–17861. [[CrossRef](#)]
8. Akpan, U.G.; Hameed, B.H. Parameters Affecting the Photocatalytic Degradation of Dyes Using TiO₂-Based Photocatalysts: A Review. *J. Hazard. Mater.* **2009**, *170*, 520–529. [[CrossRef](#)] [[PubMed](#)]
9. Kobayashi, Y.; Ishii, Y.; Yamane, H.; Watanabe, K.; Koda, H.; Kunigami, H.; Kunigami, H. Fabrication of TiO₂/Pt Core-Shell Particles by Electroless Metal Plating. *Colloids Surfaces A Physicochem. Eng. Asp.* **2014**, *448*, 88–92. [[CrossRef](#)]
10. Lei, X.F.; Xue, X.X.; Yang, H. Preparation and Characterization of Ag-Doped TiO₂ Nanomaterials and Their Photocatalytic Reduction of Cr(VI) under Visible Light. *Appl. Surf. Sci.* **2014**, *321*, 396–403. [[CrossRef](#)]
11. Cybula, A.; Nowaczyk, G.; Jarek, M.; Zaleska, A. Preparation and Characterization of Au/Pd Modified-TiO₂ Photocatalysts for Phenol and Toluene Degradation under Visible Light—The Effect of Calcination Temperature. *J. Nanomater.* **2014**, *2014*, 1–9. [[CrossRef](#)]
12. Khairy, M.; Zakaria, W. Effect of Metal-Doping of TiO₂ Nanoparticles on Their Photocatalytic Activities toward Removal of Organic Dyes. *Egypt. J. Pet.* **2014**, *23*, 419–426. [[CrossRef](#)]
13. Li, F.B.; Li, X.Z. The Enhancement of Photodegradation Efficiency Using Pt-TiO₂ Catalyst. *Chemosphere* **2002**, *48*, 1103–1111. [[CrossRef](#)]
14. Garcia-Segura, S.; Brillas, E. Applied Photoelectrocatalysis on the Degradation of Organic Pollutants in Wastewaters. *J. Photochem. Photobiol. C Photochem. Rev.* **2017**, *31*, 1–35. [[CrossRef](#)]
15. Gerlach, J.W.; Mändl, S. Correlation between RBS, Reflectometry and Ellipsometry Data for TiO₂ Films Deposited on Si. *Nucl. Instruments Methods Phys. Res. Sect. B Beam Interact. Mater. Atoms* **2006**, *242*, 289–292. [[CrossRef](#)]
16. Cao, D.; Wang, Y.; Zhao, X. Combination of Photocatalytic and Electrochemical Degradation of Organic Pollutants from Water. *Curr. Opin. Green Sustain. Chem.* **2017**, *6*, 78–84. [[CrossRef](#)]
17. Li, D.; Guo, X.; Song, H.; Sun, T.; Wan, J. Preparation of RuO₂-TiO₂/Nano-Graphite Composite Anode for Electrochemical Degradation of Ceftriaxone Sodium. *J. Hazard. Mater.* **2018**. [[CrossRef](#)] [[PubMed](#)]
18. Wang, X.; Wang, Z.; Zhang, M.; Jiang, X.; Wang, Y.; Lv, J.; He, G.; Sun, Z. Three-Dimensional Hierarchical Anatase@rutile TiO₂ Nanotree Array Films Decorated by Silver Nanoparticles as Ultrasensitive Recyclable Surface-Enhanced Raman Scattering Substrates. *J. Alloys Compd.* **2017**, *725*, 1166–1174. [[CrossRef](#)]
19. Nechache, R.; Nicklaus, M.; Diffalah, N.; Ruediger, A.; Rosei, F. Pulsed Laser Deposition Growth of Rutile TiO₂ Nanowires on Silicon Substrates. *Appl. Surf. Sci.* **2014**, *313*, 48–52. [[CrossRef](#)]
20. Yang, K.-H.; Chang, C.-M. Surface-Enhanced Raman Scattering-Active Au/TiO₂ Films Prepared by Electrochemical and Photochemical Methods. *Mater. Res. Bull.* **2013**, *48*, 372–377. [[CrossRef](#)]
21. Olvera-Rodríguez, I.; Hernández, R.; Medel, A.; Guzmán, C.; Escobar-Alarcón, L.; Brillas, E.; Sirés, I.; Esquivel, K. TiO₂/Au/TiO₂ Multilayer Thin-Film Photoanodes Synthesized by Pulsed Laser Deposition for Photoelectrochemical Degradation of Organic Pollutants. *Sep. Purif. Technol.* **2019**, *224*, 189–198. [[CrossRef](#)]

22. Graillot-Vuillecot, R.; Thomann, A.L.; Lecas, T.; Cachoncinlle, C.; Millon, E.; Caillard, A. Hot Target Magnetron Sputtering Process: Effect of Infrared Radiation on the Deposition of Titanium and Titanium Oxide Thin Films. *Vacuum* **2020**, *181*, 109734. [[CrossRef](#)]
23. Musil, J.; Baroch, P.; Vlček, J.; Nam, K.H.; Han, J.G. Reactive Magnetron Sputtering of Thin Films: Present Status and Trends. In *Thin Solid Films*; Elsevier: Amsterdam, The Netherlands, 2005; Volume 475, pp. 208–218. [[CrossRef](#)]
24. Ashfold, M.N.R.; Claeysens, F.; Fuge, G.M.; Henley, S.J. Pulsed Laser Ablation and Deposition of Thin Films. *Chem. Soc. Rev.* **2004**, *33*, 23–31. [[CrossRef](#)]
25. Rehman, S.; Ullah, R.; Butt, A.M.; Gohar, N.D. Strategies of Making TiO₂ and ZnO Visible Light Active. *J. Hazard. Mater.* **2009**, *170*, 560–569. [[CrossRef](#)]
26. Teoh, W.Y.; Mädler, L.; Amal, R. Inter-Relationship between Pt Oxidation States on TiO₂ and the Photocatalytic Mineralisation of Organic Matters. *J. Catal.* **2007**, *251*, 271–280. [[CrossRef](#)]
27. Krzanowski, J.E.; Endrino, J.L.; Nainaparampil, J.J.; Zabinski, J.S. Composite Coatings Incorporating Solid Lubricant Phases. In *Proceedings of the Journal of Materials Engineering and Performance*; Springer: Berlin/Heidelberg, Germany, 2004; Volume 13, pp. 439–444.
28. Martínez-Chávez, L.A.; Esquivel, K.; Solís-Casados, D.A.; Velázquez-Castillo, R.; Haro-Poniatowski, E.; Escobar-Alarcón, L. Nanocomposite Bi/TiO₂ Multilayer Thin Films Deposited by a Crossed Beam Laser Ablation Configuration. *Appl. Phys. A* **2021**, *127*, 1–9. [[CrossRef](#)]
29. González-Zavala, F.; Escobar-Alarcón, L.; Solís-Casados, D.A.; Rebollar, D.A.; Basurto, R.; Haro-Poniatowski, E. Deposition and Photocatalytic Activity of Ag: V₂O₅ Thin Films. In *Proceedings of the Materials Research Society Symposium Proceedings*; Materials Research Society, Cancún, México, 1 June 2016; Volume 1817, pp. 22–27.
30. Gonzalez-Zavala, F.; Escobar-Alarcón, L.; Solís-Casados, D.A.; Rivera-Rodríguez, C.; Basurto, R.; Haro-Poniatowski, E. Preparation of Vanadium Oxide Thin Films Modified with Ag Using a Hybrid Deposition Configuration. *Appl. Phys. A Mater. Sci. Process.* **2016**, *122*, 1–6. [[CrossRef](#)]
31. Hernández, R.; Hernández-Reséndiz, J.R.; Cruz-Ramírez, M.; Velázquez-Castillo, R.; Escobar-Alarcón, L.; Ortiz-Frade, L.; Esquivel, K. Au-TiO₂ Synthesized by a Microwave- and Sonochemistry-Assisted Sol-Gel Method: Characterization and Application as Photocatalyst. *Catalysts* **2020**, *10*, 1052. [[CrossRef](#)]
32. Kimura, K.; Naya, S.; Jin-nouchi, Y.; Tada, H. TiO₂ Crystal Form-Dependence of the Au/TiO₂ Plasmon Photocatalyst's Activity. *J. Phys. Chem. C* **2012**, *116*, 7111–7117. [[CrossRef](#)]
33. Lee, K.M.; Lee, D.J.; Ahn, H. XRD and TEM Studies on Tin Oxide (II) Nanoparticles Prepared by Inert Gas Condensation. *Mater. Lett.* **2004**, *58*, 3122–3125. [[CrossRef](#)]
34. Scipioni, R.; Gazzoli, D.; Teocoli, F.; Palumbo, O.; Paolone, A.; Ibris, N.; Brutti, S.; Navarra, M.A. Preparation and Characterization of Nanocomposite Polymer Membranes Containing Functionalized SnO₂ Additives. *Membranes* **2014**, *4*, 123–142. [[CrossRef](#)]
35. Zheng, X.; Qiao, X.; Luo, F.; Wan, B.; Zhang, C. Low-Cost High- Performance NO₂ Sensor Based on Nanoporous Indium Tin Oxide (ITO) Film. *Sensors Actuators B Chem.* **2021**, *346*, 130440. [[CrossRef](#)]
36. Theivasanthi, T.; Alagar, M. *Titanium Dioxide (TiO₂) Nanoparticles-XRD Analyses-An Insight*; arXivLabs; Cornell University: Ithaca, NY, USA, 2013.
37. Rodrigues, M.S.; Borges, J.; Gabor, C.; Munteanu, D.; Apreutesei, M.; Steyer, P.; Lopes, C.; Pedrosa, P.; Alves, E.; Barradas, N.P.; et al. Functional Behaviour of TiO₂ Films Doped with Noble Metals. *Surf. Eng.* **2016**, *32*, 554–561. [[CrossRef](#)]
38. Mote, V.; Purushotham, Y.; Dole, B. Williamson-Hall Analysis in Estimation of Lattice Strain in Nanometer-Sized ZnO Particles. *J. Theor. Appl. Phys.* **2012**, *6*, 6. [[CrossRef](#)]
39. Khorsand Zak, A.; Abd Majid, W.H.; Abrishami, M.E.; Yousefi, R. X-Ray Analysis of ZnO Nanoparticles by Williamson-Hall and Size-Strain Plot Methods. *Solid State Sci.* **2011**, *13*, 251–256. [[CrossRef](#)]
40. Jing, Z.; Meijun, L.; Zhaochi, F.; Jun, C.; Li, C. UV Raman Spectroscopic Study on TiOI. Phase Transformation at the Surface and in the Bulk. *J. Phys. Chem. B* **2006**, *110*, 927–935. [[CrossRef](#)]
41. Leyva-Porras, C.; Toxqui-Teran, A.; Vega-Becerra, O.; Miki-Yoshida, M.; Rojas-Villalobos, M.; García-Guaderrama, M.; Aguilar-Martínez, J.A. Low-Temperature Synthesis and Characterization of Anatase TiO₂ Nanoparticles by an Acid Assisted Sol-Gel Method. *J. Alloys Compd.* **2015**, *647*, 627–636. [[CrossRef](#)]
42. Huang, X.; El-Sayed, M.A. Gold Nanoparticles: Optical Properties and Implementations in Cancer Diagnosis and Photothermal Therapy. *J. Adv. Res.* **2010**, *1*, 13–28. [[CrossRef](#)]
43. Jung, H.Y.; Yeo, I.S.; Kim, T.U.; Ki, H.C.; Gu, H.B. Surface Plasmon Resonance Effect of Silver Nanoparticles on a TiO₂ Electrode for Dye-Sensitized Solar Cells. *Appl. Surf. Sci.* **2018**, *432*, 266–271. [[CrossRef](#)]
44. Wisniewska, J.; Guesmi, H.; Ziolk, M.; Tielens, F. Stability of Nanostructured Silver-Platinum Alloys. *J. Alloys Compd.* **2019**, *770*, 934–941. [[CrossRef](#)]
45. Kernazhitsky, L.; Shymanovska, V.; Gavrilko, T.; Naumov, V.; Fedorenko, L.; Kshnyakin, V.; Baran, J. Room Temperature Photoluminescence of Anatase and Rutile TiO₂ Powders. *J. Lumin.* **2014**, *146*, 199–204. [[CrossRef](#)]
46. Abazović, N.D.; Čomor, M.I.; Dramićanin, M.D.; Jovanović, D.J.; Ahrenkiel, S.P.; Nedeljković, J.M. Photoluminescence of Anatase and Rutile TiO₂ Particles. *J. Phys. Chem. B* **2006**, *110*, 25366–25370. [[CrossRef](#)]
47. Chen, C.C.; Lu, C.S.; Chung, Y.C.; Jan, J.L. UV Light Induced Photodegradation of Malachite Green on TiO₂ Nanoparticles. *J. Hazard. Mater.* **2007**, *141*, 520–528. [[CrossRef](#)]

48. Ju, Y.; Qiao, J.; Peng, X.; Xu, Z.; Fang, J.; Yang, S.; Sun, C. Photodegradation of Malachite Green Using UV-Vis Light from Two Microwave-Powered Electrodeless Discharge Lamps (MPEDL-2): Further Investigation on Products, Dominant Routes and Mechanism. *Chem. Eng. J.* **2013**, *221*, 353–362. [[CrossRef](#)]
49. Liu, X.; An, S.; Shi, W.; Yang, Q.; Zhang, L. Microwave-Induced Catalytic Oxidation of Malachite Green under Magnetic Cu-Ferrites: New Insight into the Degradation Mechanism and Pathway. *J. Mol. Catal. A Chem.* **2014**, *395*, 243–250. [[CrossRef](#)]
50. Qin, J.; Ye, S.; Yan, K.; Zhang, J. Visible Light-Driven Photoelectrocatalysis for Simultaneous Removal of Oxytetracycline and Cu (II) Based on Plasmonic Bi/Bi₂O₃/TiO₂ Nanotubes. *J. Colloid Interface Sci.* **2022**, *607*, 1936–1943. [[CrossRef](#)]
51. Matarrese, R.; Mascia, M.; Vacca, A.; Mais, L.; Usai, E.; Ghidelli, M.; Mascaretti, L.; Bricchi, B.; Russo, V.; Casari, C.; et al. Integrated Au/TiO₂ Nanostructured Photoanodes for Photoelectrochemical Organics Degradation. *Catalysts* **2019**, *9*, 340. [[CrossRef](#)]
52. Orimolade, B.O.; Zwane, B.N.; Koiki, B.A.; Tshwenya, L.; Peleyeju, G.M.; Mabuba, N.; Zhou, M.; Arotiba, O.A. Solar Photoelectrocatalytic Degradation of Ciprofloxacin at a FTO/BiVO₄/MnO₂ Anode: Kinetics, Intermediate Products and Degradation Pathway Studies. *J. Environ. Chem. Eng.* **2020**, *8*, 103607. [[CrossRef](#)]
53. Daskalaki, V.M.; Fulgione, I.; Frontistis, Z.; Rizzo, L.; Mantzavinos, D. Solar Light-Induced Photoelectrocatalytic Degradation of Bisphenol-A on TiO₂/ITO Film Anode and BDD Cathode. *Catal. Today* **2013**, *209*, 74–78. [[CrossRef](#)]
54. Solís-Casados, D.A.; Escobar-Alarcón, L.; Fernández, M.; Valencia, F. Malachite Green Degradation in Simulated Wastewater Using Nix:TiO₂ Thin Films. *Fuel* **2013**, *110*, 17–22. [[CrossRef](#)]
55. Mohite, V.S.; Mahadik, M.A.; Kumbhar, S.S.; Hunge, Y.M.; Kim, J.H.; Moholkar, A.V.; Rajpure, K.Y.; Bhosale, C.H. Photoelectrocatalytic Degradation of Benzoic Acid Using Au Doped TiO₂ Thin Films. *J. Photochem. Photobiol. B Biol.* **2015**, *142*, 204–211. [[CrossRef](#)] [[PubMed](#)]
56. Sreedhar, A.; Reddy, I.N.; Kwon, J.H.; Yi, J.; Sohn, Y.; Gwag, J.S.; Noh, J.S. Charge Carrier Generation and Control on Plasmonic Au Clusters Functionalized TiO₂ Thin Films for Enhanced Visible Light Water Splitting Activity. *Ceram. Int.* **2018**, *44*, 18978–18986. [[CrossRef](#)]
57. Landolsi, Z.; Ben Assaker, I.; Nunes, D.; Fortunato, E.; Martins, R.; Chtourou, R.; Ammar, S. Enhanced Electrical and Photocatalytic Properties of Porous TiO₂ Thin Films Decorated with Fe₂O₃ Nanoparticles. *J. Mater. Sci. Mater. Electron.* **2020**, *31*, 20753–20773. [[CrossRef](#)]
58. Díaz-Real, J.A.; Ma, J.; Alonso-Vante, N. Highly Photoactive Brookite and Anatase with Enhanced Photocatalytic Activity for the Degradation of Indigo Carmine Application. *Appl. Catal. B Environ.* **2016**, *198*, 471–479. [[CrossRef](#)]